

Morphology evolution of the light trapping structure using atmospheric plasma textured c-Si wafer for silicon solar cells

Cite as: J. Appl. Phys. 130, 023105 (2021); doi: 10.1063/5.0044508

Submitted: 17 January 2021 · Accepted: 24 June 2021 ·

Published Online: 14 July 2021



View Online



Export Citation



CrossMark

Peng Zhang, Jie Wu, Hengxi Tian, Yuqing Dong, and Deping Yu^{a)}

AFFILIATIONS

School of Mechanical Engineering, Sichuan University, Chengdu 610065, China

Note: This paper is part of the Special Topic on Fundamentals and Applications of Atmospheric Pressure Plasmas.

^{a)}**Author to whom correspondence should be addressed:** williamydp@scu.edu.cn

ABSTRACT

Applying atmospheric plasma etching to the surface texturing process of silicon solar cells is a promising strategy for the current photovoltaic manufacturing industry due to its low equipment cost and good fabrication flexibility. This paper investigates the morphology evolution of the silicon surface etched by an Ar/CF₄/O₂ plasma and the associated optical properties. Results show that the generation of the light trapping structure on the polished silicon surface can be divided into two stages on the basis of the multi-scale morphological images and the quantitative evaluation of roughness parameters. The initial roughening stage mainly involves the formation of high-frequency nanoroughness that can act as an effective medium layer with a gradual refractive index. The resulting optical medium effect can reduce the surface reflectance within a broad range of wavelengths. At the next texturing stage, the low-frequency and high-amplitude microroughness dominates the morphology of the etched silicon surface. It features inverted parabolic structures with a high aspect ratio, which can cause multiple reflections of the incident light. The optical medium effect resulting from the nanoroughness is also inherited. Thus, the anti-reflectance property of the etched silicon surface is greatly improved. This work demonstrates that the light trapping properties of silicon surface etched by atmospheric plasma jet are a synergy of the optical medium effect and geometrical optics. Insights into the morphology evolution and optical properties of the textured surfaces are important for developing a new surface texturing process of silicon solar cells.

Published under an exclusive license by AIP Publishing. <https://doi.org/10.1063/5.0044508>

I. INTRODUCTION

Silicon solar cells are still the optimal choice for large-scale photovoltaic applications because of their low manufacturing cost and acceptable photovoltaic conversion efficiency although thin-film and perovskite solar cells have great prospects for development in the future.^{1,2} In particular, since the production costs of a single crystalline silicon (c-Si) material have been greatly reduced, developing surface texturing technologies with high efficiency and low costs will be an important breakthrough in enhancing the light trapping capability of silicon substrates. It aims to provide further room for improvement in terms of photovoltaic conversion efficiency and reduction in manufacturing costs.^{3–5}

At present, traditional wet etching with an alkaline solution is not an ideal choice due to the negative effect of backside texturing on the quality of dielectric rear surface passivation and the

environmental issue caused by the large amount of polluting waste liquid.⁶ By contrast, dry etching with plasma can produce “black silicon” that possesses nanotextured surfaces, which results in an extremely low reflectance and a continuously improving passivation.^{7–9} After passivation by plasma-assisted atomic layer deposition of Al₂O₃, an effective surface recombination rate of less 15 cm/s can be obtained.¹⁰ This means a better collection capability of light-generated carriers than the current passivated emitter and rear cell that has a surface recombination rate of 20–270 cm/s. Thus, newly developed texturing technologies based on vacuum reactive ion etching (RIE) have attracted much attention.^{11,12} However, low-pressure plasma etching techniques performing in a vacuum chamber have only a small throughput related to plasma chemistry.¹³ In the absence of a sufficiently high etch rate, the needs of mass production cannot be satisfied. The use of a vacuum chamber also increases the equipment cost and restricts the wafer

size, thereby greatly limiting engineering applications.^{14,15} In contrast to RIEs, atmospheric-pressure plasma texturing technology, which can provide abundant F radicals in air, presents greater development potential in terms of equipment cost and process flexibility.^{16,17}

Producing a desired light trapping structure on one side by plasma etching is the key to a texturing process for silicon solar cells.^{18,19} Fluorine-containing plasma can etch Si-based materials via chemical reactions with Si atoms or the bombardment of neutral ions.^{20–22} Affected by the micro-mask effect and material anisotropy, such as the local coverage of the by-product with etch resistance and the difference in chemical reaction rates in crystal orientation, the etched silicon surface is displayed as non-periodic microstructures with a certain correlation length.^{23,24} This etching process is known as plasma texturing. The crowded pyramid structure is a common morphology feature on textured silicon surfaces, and it can be achieved through alkaline solution wet etching and plasma dry etching.^{25,26} The average surface reflectivity can decrease to below 12% in the absence of post-treatments because the micrometer-level pyramid structures lead to multiple reflections of the incident light in the wafer.²⁷ Similarly, an inverted pyramid structure allows incident light to have abundant reflections inside the microstructure. Its surface reflectivity can decrease to 6.4% in the case of a high aspect ratio.²⁸ Moreover, a textured surface with needle-like and round-top structures can be obtained using SF₆/O₂ gas mixtures in maskless RIE etching.²⁹ The two microstructures can reduce the surface reflectance of silicon solar cells and even obtain good light trapping properties. However, given that the feature sizes of the needle-like or round-top structure are usually only at the nanoscale, the available wavelength range (350–1100 nm) of the incident light nearly exceeds the maximum gap between microstructural peaks; as a result, the light is prevented from entering the textured surface.¹³ Geometrical optics are not the major reason for the reduction in surface reflectance. In this case, the nanoscale structures of the textured surface can be viewed as an effective medium layer with a gradual refractive index from air to silicon, and it decreases the reflectivity in a broad wavelength range and enables the etched surface to obtain black silicon properties.³⁰ The change in the equivalent refractive index determined by microstructural features and nanoroughness considerably affects the reflectivity of textured surfaces.^{12,31} Therefore, capturing and analyzing the static geometrical parameters (e.g., microstructural feature size and height distribution) of textured silicon surfaces are important to understand the generation mechanism of light trapping properties.

The etching behaviors of silicon surfaces become complicated and diverse because of the altered plasma generating parameters or work conditions.^{31–33} Clarifying the evolution of etching morphology and its dependence on process parameters is crucial for the development of new texturing techniques. For a low-pressure cryogenic RIE process, the model proposed by David *et al.* describes a self-shadowing effect that is based on a dynamic process. This process involves silicon etching, masking layer growth, and masking layer removal, and it depends on a synthetic effect of radical diffusion and ion bombardment influenced by process parameters (e.g., mixed gas content, substrate temperature, and voltage bias). It can explain the initial formation of black silicon

nanostructures and the subsequent morphology evolution.³¹ However, the ion energy and active radical concentration of atmospheric-pressure plasma have an obvious difference from those of low-pressure plasma.^{14,34} The downstream plasma interacts with the silicon surface when the etching is conducted by a jet.³⁵ The difference in environmental atmosphere and plasma temperature may exert unknown influences on micro-mask effects and etching anisotropy. Without ion acceleration by voltage bias, the weak physical bombardment may reduce the desorption of by-products at the reaction interface, thereby promoting the micro-mask effect. At atmospheric pressure, the plasma jet with a relatively high temperature (above room temperature) may facilitate the interfacial chemical reaction, which alters the anisotropy of plasma etching. However, current studies on micro-/nano-scale morphologies of atmospheric plasma etching silicon surfaces are relatively scarce. These studies have focused only on the dependence of etching rate and surface roughness on process parameters or reported the formation of unique microstructures on the etched silicon surface.^{20,21} The different diffusion and transport mechanisms during atmospheric plasma texturing must be considered due to the sensitivity of the deposition and desorption of the masking layer (SiO_xF_y) to the substrate temperature and environmental pressure.³⁶ The microstructural formation and the morphology evolution of the silicon wafer textured by atmospheric plasma etching are not well understood. Therefore, the formation and the morphology evolution of the light trapping structure during atmospheric plasma texturing should be clarified for the development of new texturing processes for silicon solar cells.

This study is the first to apply atmospheric plasma jet to the surface texturing process for silicon solar cells. The focus is on the morphology evolution of the silicon surface etched by an Ar/CF₄/O₂ plasma and the associated roughness parameters. The relations between the light trapping properties and morphology evolution of the textured surface are expounded in detail by characterizing the multi-scale morphology features in terms of height and spatial correlation.

II. MATERIALS AND DEVICES

Surface texturing processes in the industry usually begin from diamond wire sawn silicon wafers.³⁷ However, the polished p-type Si (100) wafers (Suzhou Research Materials Microtech Co., CHN) with a thickness of 0.6 mm and a resistivity below 0.01 Ω cm were used for atmospheric plasma texturing experiments in this work to accurately capture the morphology evolution of the etched surfaces accurately. A native oxide layer with around 0.8 nm thickness that occurs on as-received silicon wafer³⁸ can be ignored because it is very thin and easily etched. In addition, the root mean square (RMS) roughness over a 50 × 50 μm² area was measured to be nearly 0.3 nm by using an atomic force microscope (AFM).

Atmospheric plasma texturing was conducted using a home-made inductively coupled plasma (ICP) jet device mounted on a three-axis machine. The ICP system used Ar and CF₄/O₂ as the working and etching gases, respectively, which can be excited by the high-frequency electromagnetic field to generate plasma containing F and O radicals. As shown in Fig. 1, the Ar/CF₄/O₂ gas mixture was passed into a ceramic tube with a constant flow rate of

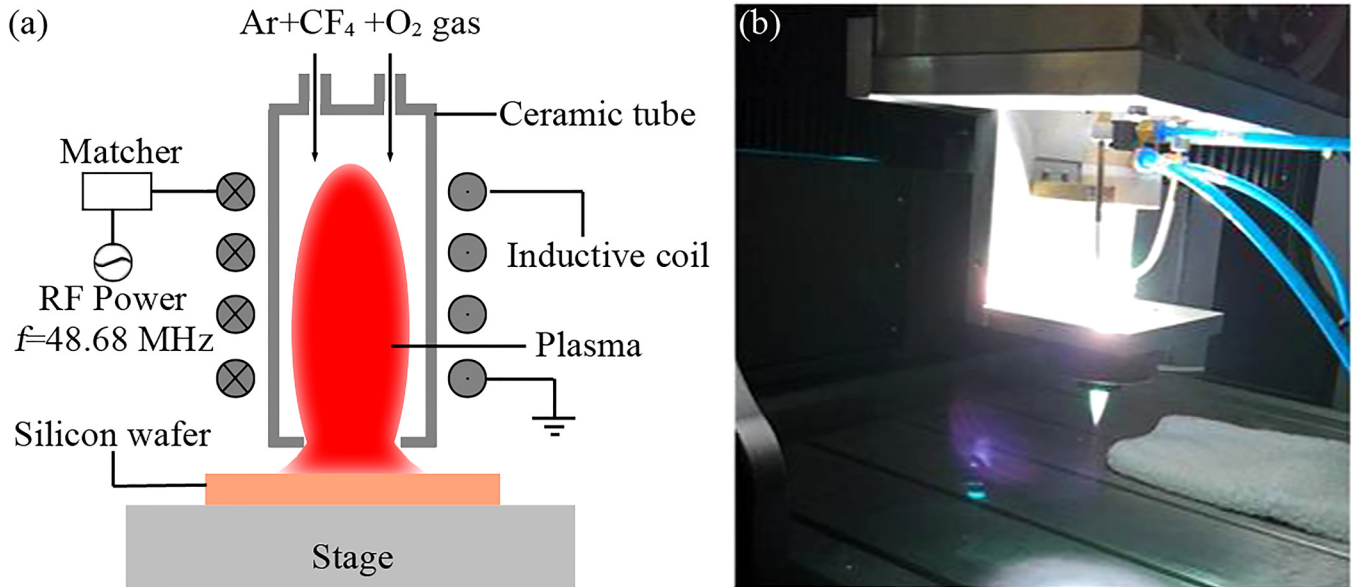


FIG. 1. (a) Schematic and (b) photo of the atmospheric ICP jet device mounted on a three-axis machine.

Ar (700 sccm), CF₄ (11 sccm), and O₂ (2 sccm) via mass flow controllers (LF420-S). The fluorine-containing plasma was generated inside the inductive coil and sprayed out from a nozzle with 12 mm diameter driven by a 40.68 MHz radio frequency (RF) power source (RSGK 2000) and an automatic matcher (PSGK-IIIA). A water-cooling system involving the sample stage and an inductive coil was always kept on, and the RF power was fixed at 1100 W to ensure the stability of the plasma jet. The jet length can reach approximately 20 mm under a given optimal parameter condition. The jet temperature at the axial center position of 10 mm away from the nozzle outlet was close to 1000 K, as determined via thermocouple probe measurement.³⁹ The chemical components of the plasma jet were detected by an optical emission spectrometer (Ocean optics MX2500+, USA). In Fig. 2, the emission lines of Ar atoms at 750.4, 763.5, 794.8, 801.4, 811.5, and 912.3 nm, F atoms at 739.9 and 775.5 nm, and O atoms at 844.6 nm are well marked. The emission lines of C₂ molecules at 471.5, 516.5, 558.5, and 563.5 nm can be observed in the optical emission spectrum. These results indicate that the atmospheric ICP jet containing a mass of active radicals (F and O) possessed the capability to etch c-Si.

III. EXPERIMENT AND ANALYSIS

The texturing experiments were conducted in the atmosphere by using the ICP jet device to acquire the light trapping structure on the c-Si surface. A Si sample of 2 × 2 cm² was fixed on the sample stage after being cleaned through sanitation in ethanol and de-ionized water. Driven by the three-axis machine, the stable-operating ICP jet arrived at a position of 10 mm above the sample stage and then performed a reciprocating scanning of 15 mm length at a velocity of 5 mm/s to homogenize the etching

effect on the entire sample surface. The working parameters of ICP remained constant and only the etch time was increased from 0.5 to 10 min when investigating the morphology evolution of the atmospheric plasma etching silicon surface. During the texturing process, the surface temperature of the silicon sample was monitored with an infrared imaging camera (R300W2 R15, NEC Avio Infrared Technologies Co., Japan). As shown in Fig. 3, the silicon surface temperature at point A fluctuated only between 180 and 250 °C after the sample was heated rapidly. Therefore, the etched interface temperature was relatively stable.

The 2D surface morphology of the etched silicon surface was evaluated quickly by using an optical microscope (GX51,

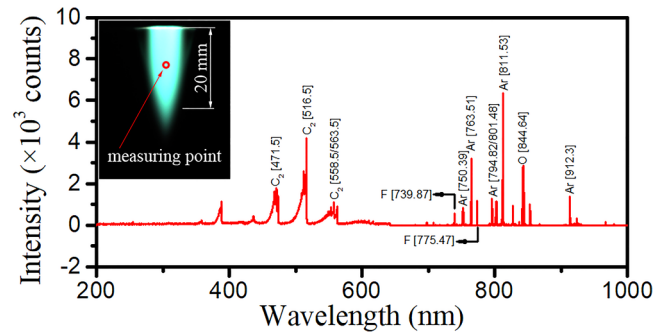


FIG. 2. Optical emission spectrum of atmospheric ICP jet at the axial center position of 10 mm away from the nozzle outlet. The inset shows a photo of the atmospheric ICP jet.

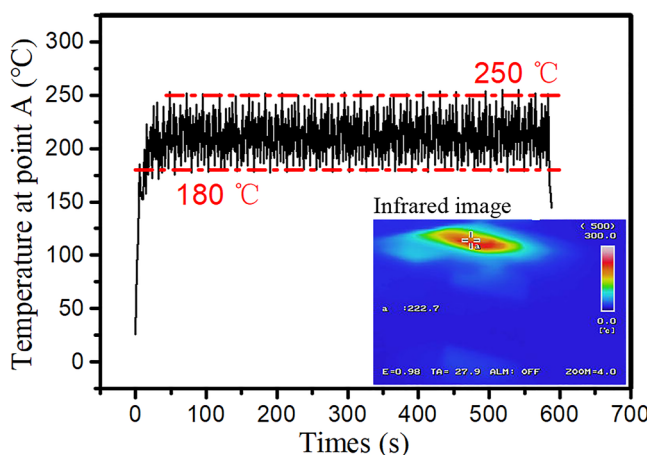


FIG. 3. Temperature change on the silicon sample surface during atmospheric ICP texturing.

OLYMPUS, Japan). Detailed studies of 3D microscopic morphology associated with several statistical quantities and the profile and size of the light trapping structure were performed with an AFM (SPI3800N, Seiko, Japan) and a scanning electron microscope (SEM, Inspect F50, FEI, USA). For instance, the height distribution of the textured surface, the height-height correlation function, and the power spectral density (PSD) were extracted from an AFM data image by using the open-source “Gwyddion” software.⁴⁰ Microstructural features were measured using the SEM image collected from the cross sections of the sample. The total (diffuse and specular) reflectivity (R) of the sample surface in the wavelength range of 400–1100 nm and the transmittivity (T) through the wafer were measured with a spectrophotometer with an integrating sphere (UV3600, Shimadzu Corporation, Japan). As a reference, the polished Si wafer and an alkaline textured Si wafer were used for optical measurements. The alkaline texturing process was conducted by immersing the oxide-free Si wafer in 10 wt. % KOH solution for 30 min at a constant temperature of 70 °C.

IV. RESULTS AND DISCUSSION

A. Morphology evolution of the atmospheric plasma etching silicon surface

An optical microscope can obtain the 2D surface morphology within a large scope. Figure 4 displays the typical morphology features of the silicon surface at different etching times. In the initial 0.5 min, the smooth silicon surface gradually formed several tiny pores. As the etch time increased from 1 to 2.5 min, large pores began to appear, and almost the whole area was covered. This stage can be considered a surface roughening process, during which the initial surface is not completely etched yet. However, micropores gradually merged and formed spherical pits as the etch time further increased. The maximum diameter of these spherical pits increased to 10 μm from hundreds of nanometers within a few minutes. At this stage, the surface material of silicon was removed

rapidly, and a uniformly distributed microstructure emerged on the etched surface. This result suggests that the etched silicon surface is likely to form a micrometer-scale parabolic structure instead of a pyramid structure when the atmospheric plasma jet is utilized for texturing under the given parameter condition.

An AFM mounted with a Si_3N_4 tip of 20 nm radius was used to draw 3D images of the silicon etched surface to present the nano-scale morphology evolution intuitively. Figure 5 shows the microscopic morphology characteristics and height distributions of the silicon surface etched for different etching times. The initially formed micropores had a depth of only 250 nm, and the distribution intervals far exceeded their own dimensions. As the etch time increased, the depth and the width of the pores gradually increased until the original surface was completely occupied by micropores. In the first 2.5 min, the peak of the height distribution density was always at the zero position. Only a one-sided tail was enlarged gradually, which was accompanied with a decline in the peak value. This can be confirmed as a quick roughening process during which the smooth silicon surface was etched by the atmospheric plasma jet. Subsequently, the etched surface consisting of the micropores was further textured and formed the inverted parabolic structure consisting of spherical pits. Obviously, the size of the pits increased as the etch time progressed. However, the measuring depth of spherical pits did not continue to increase as much as their width did because the top material of the formed pits began to be removed. The peak of the height distribution function left the zero position, and the distribution became relatively uniform in a wide range. Therefore, the spherical pits of the etched surface were well distributed. The second stage can be regarded as a growing process of the textured surface during which the micrometer-scale parabolic structure can be achieved.

B. Quantitative evaluation of the etched surface morphology

The microstructures of textured silicon surfaces are usually described as a pyramid or inverted pyramid structure and a round-top or columnar-like one.^{25,29} Providing quantitative information on the etched surface morphology is important because of its sensitivity to the alteration in surface morphology.⁴⁰ Analysis of the roughness parameters can contribute to a detailed understanding of the formation and evolution of the light trapping structure.¹³ The statistics on the depth, width, and aspect ratio of the pores and pits formed by plasma etching in Fig. 6(a) show that the etching of the smooth silicon surface by atmospheric plasma jet could be divided into two stages. In the initial roughening process, the depth of the micropores was determined by the maximum etching depth, which was equal to the distance from the original surface to the bottom of the micropores. The depth, width, and aspect ratio of the micropores rapidly increased. An abrupt change in curve occurred when the critical point was reached, where a mass of pores covered the original surface and began to merge and form large spherical pits. The aspect ratio of the spherical pits decreased sharply from 0.35 to 0.1 due to the increasing chord length but declining chord height. This condition signaled the beginning of the second stage, namely, the growing process of the textured surface. The width of the spherical pits at this stage was constantly

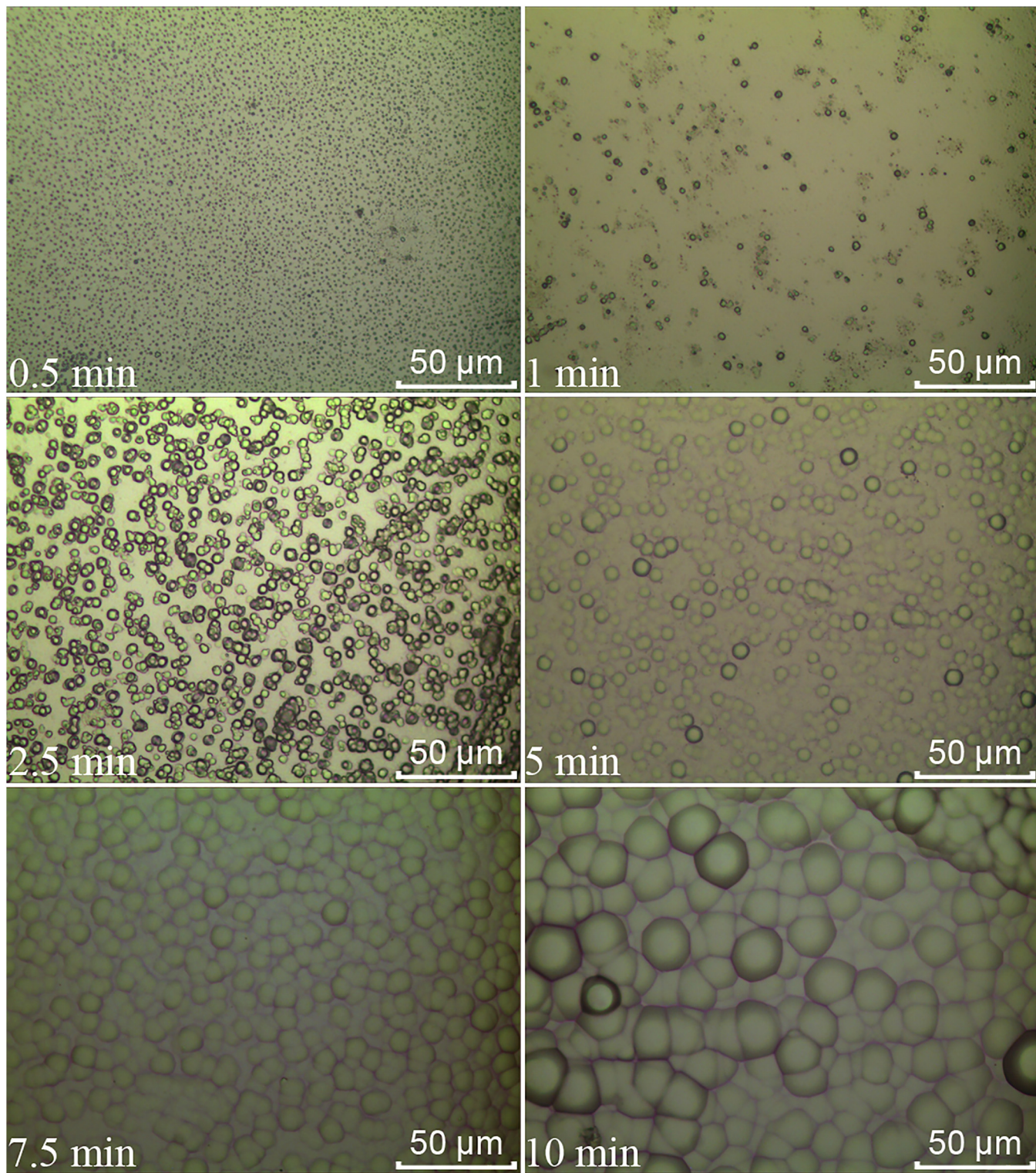


FIG. 4. Optical microscope images of the silicon surface etched for different times by using atmospheric plasma jet.

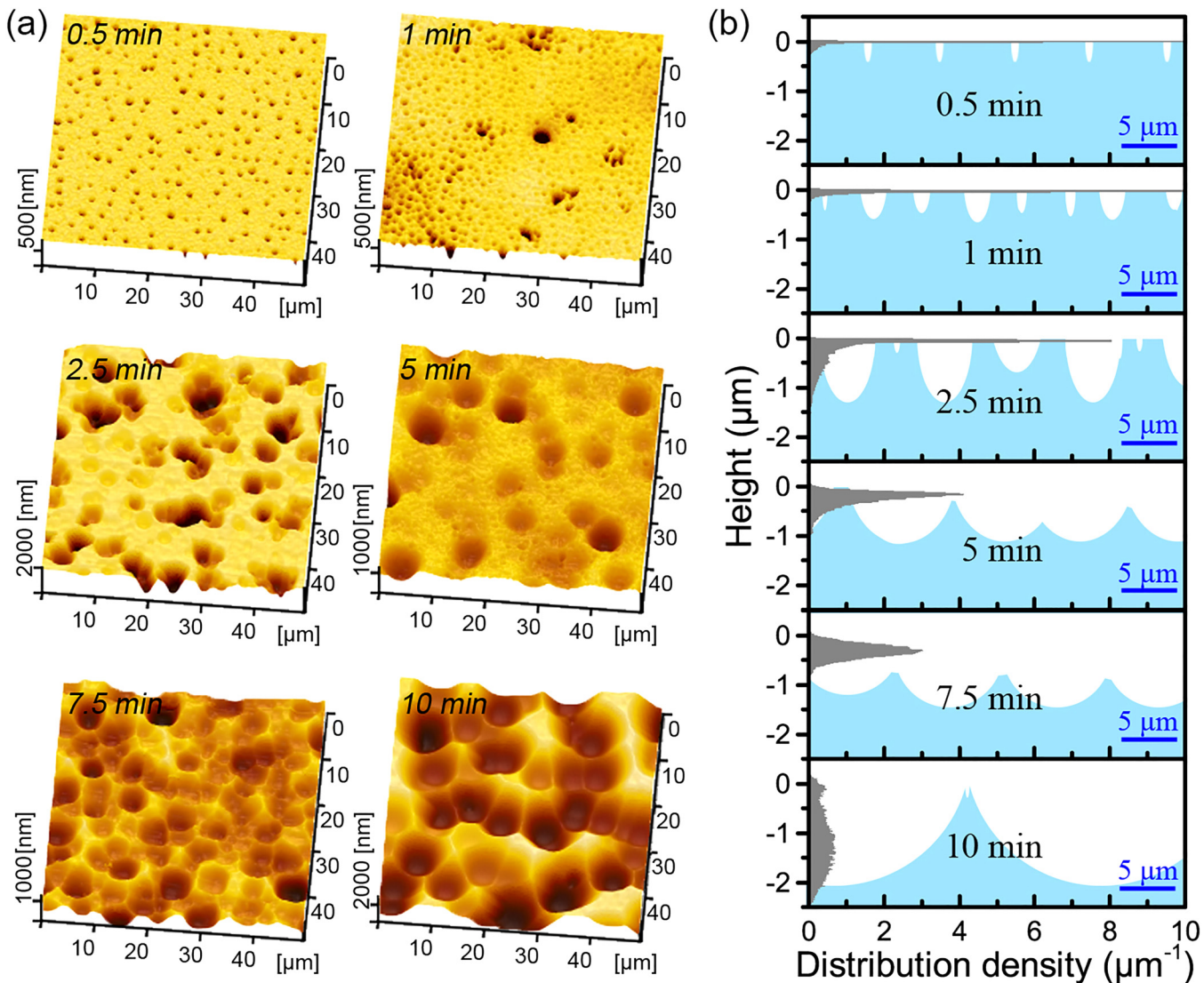


FIG. 5. (a) AFM images collected from the etched silicon surfaces and (b) the corresponding height distribution functions. The inserted blue backgrounds show the profile characteristics of the etched silicon surface. The vertical scale is the same as the axis of the height. The horizontal scale is marked as deep blue.

expanding, but the increase in depth was limited because chord height was determined by the difference in etching rate between the top and bottom. The same microstructural feature was maintained after etching for 10 min. Thus, the chord length of the largest spherical pit exceeded 10 μm but its chord height was still not more than 2 μm. The amplitude parameters acquired from 50 × 50 μm² AFM images, including RMS roughness, skewness (S_{sk}), and kurtosis (S_{ku}), were also used to describe the morphology evolution of the etched surface. As shown in Fig. 6(b), the RMS roughness curve of the etch surface showed a phased rising tendency but was non-continuous, which corresponded exactly to the

two stages of roughening (I) and texturing (II). S_{sk} , which indicates the asymmetry of the height distribution function,⁴⁰ rapidly transitioned from a negative value to zero. Therefore, the proportion of the etched areas in which the material removal occurred gradually reached 100% in the initial roughening process. At the texturing stage, the newly exposed reaction interface continued to extend downward. Similarly, S_{ku} , which reflects the sharpness of the distribution peak and the flatness of its tails,⁴⁰ transitioned from a positive value to zero. Therefore, the local etching was not uniform but the holistic distribution of the surface heights became relatively uniform with the further increase in roughness.

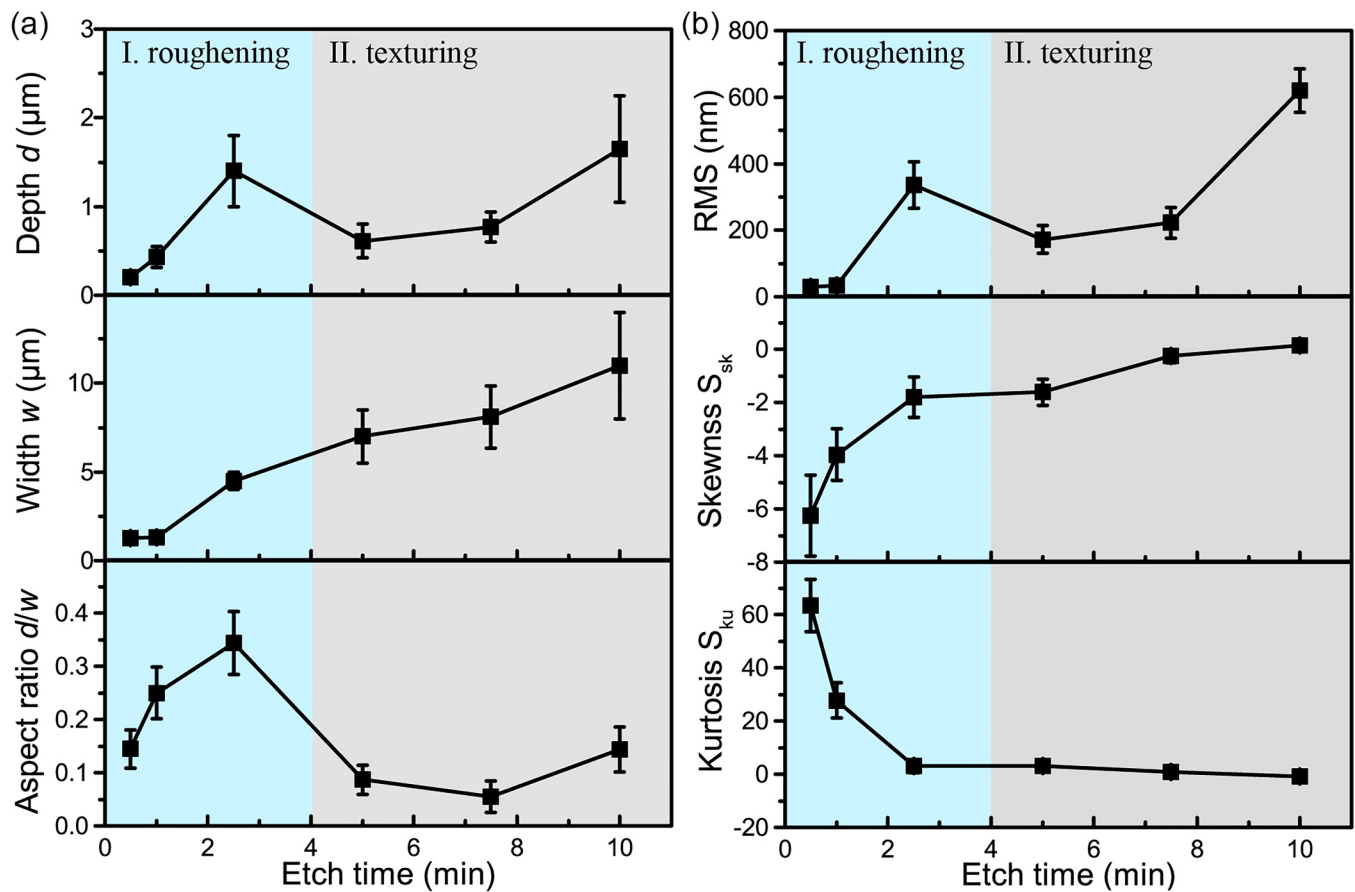


FIG. 6. Changes in (a) microstructural size and (b) roughness parameters etched for different times by using atmospheric plasma jet.

Aside from the vertical fluctuations of surface height, the spatial correlation or periodicity of the etching-formed microstructure should also be described. As shown in Fig. 7(a), the correlation length (ξ) and the roughness exponent (α) determined by the height-height correlation functions $H(r)$ of the etched surface can be obtained with the local fitting curve.⁴¹ The $H(r)$ curves of the silicon surfaces etched for 0.5 and 10 min were plotted to illustrate the extraction of the parameters. RMS roughness (rms), which is equal to the root of $0.5 \cdot H(\infty)$, was completely consistent with the previous results. The roughness exponent (α) is half the slope of the linear increasing part of the log-log plot of $H(r)$, which increased from 0.61 to 1.22 with the etch time. This finding indicates that the contribution of the high-frequency fluctuations to surface roughness gradually declined. Correlation length (ξ) reflects the density of surface fluctuations. The increasing value (from 549 to 4363 nm) implies that the region inside where the surface heights are correlated increased with etching time. The two parameters confirm that the feature size and the distribution period of the light trapping structure increased as etching continued. PSD can be used to analyze the intensity of morphology components in

the spatial frequency domain.⁴² Figure 7(b) shows the radial PSD function of the silicon surface etched for different times, as calculated by the Fourier transform of the 3D surface height distribution. At the initial stage, the surface fluctuations of the etched silicon were dominated by a high frequency and a low amplitude (small roughness). However, as etching continued, low-frequency fluctuations nearly absolutely dominated the morphology characteristic of the etched surface, especially after entering the second stage (etching time of over 2.5 min).

C. Optical properties of the textured surface using atmospheric plasma jet

The low reflectance of silicon surface is mainly attributed to geometrical optics and the optical medium effect resulting from various microstructures.^{9,12,13} The shape feature, size, and distribution of microstructure exert an important effect on the optical properties of the textured surface. In this study, the total reflectivity (R) of the silicon surface etched for different times was measured in the wavelength range of 400–1100 nm to identify an optimized

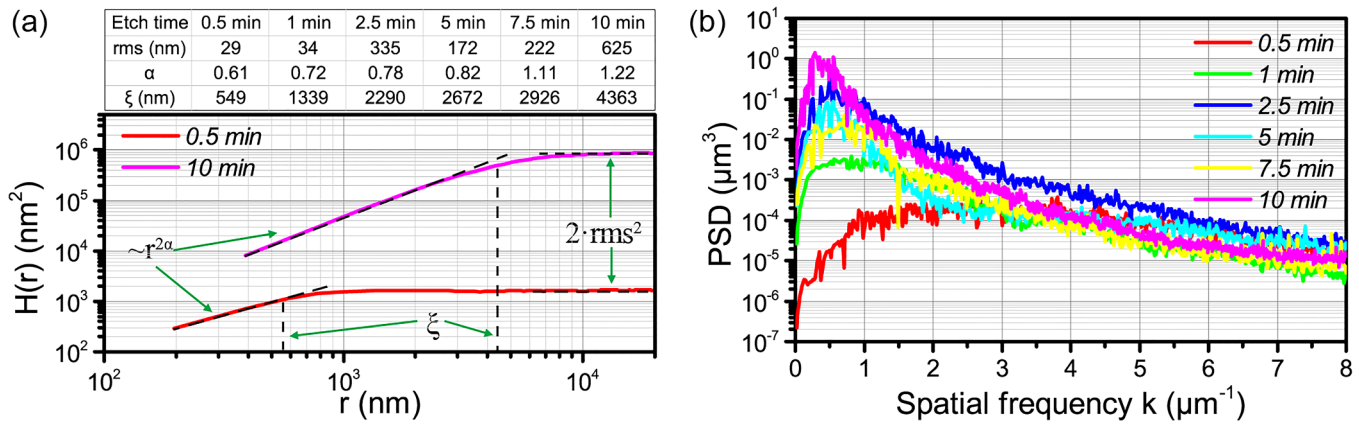


FIG. 7. (a) Height-height correlation function and (b) radial PSD function of the etched silicon surface. The RMS roughness (rms), the correlation length (ξ), and the roughness exponent (α) labeled on the $H(r)$ curves for 0.5 and 10 min. $H(\infty) = 2 \cdot \text{rms}^2$; $H(\xi) = (1 - 1/e) \cdot H(\infty)$; $H(r) \sim r^{2\alpha}$.

textured structure for making high-efficiency silicon solar cells. The reflectance spectra of the polished Si wafer and a KOH-textured wafer were also measured as a reference. In accordance with the measured transmittivity (T), the absorptivity (A) around 1100 nm that is close to the silicon bandgap can be calculated with the equation $A = 1 - R - T$. For a comparison with the optical response of the inverted parabolic structure, the absorptance in the theoretical Yablonovitch limit is also plotted according to the formula⁴³

$$A_{\text{Yabl}} = 1 - \frac{1}{1 + 4n_{\text{Si}}^2 a_{\text{Si}} t},$$

where n_{Si} is the refractive index of silicon, a_{Si} is the absorption coefficient of silicon,⁴⁴ and t is the wafer thickness.

As shown in Fig. 8, the measured surface reflectivity was relatively high (30%–40%) at the beginning of plasma etching (less

than 1 min). Only a slight improvement was observed compared with the polished surface. The reason is that most areas of the etched silicon were dominated by the polished surface. Only a few micropores appeared, and their feature size was very small that they could not be resolved by the incident light. Moreover, the high-frequency roughness was less than 40 nm, which indicates the absence of an effective transition with an increasing refractive index from air to silicon in the depth direction. As a result, the optical medium effect of the silicon surface was negligible. However, when the etch time increased to 2.5 min, the micropores occupied the entire etched surface. At this time, surface roughness was determined by the high-frequency fluctuations and reached a relatively high value (RMS of 335 nm). It could act as an effective medium layer with a thickness of approximately 400 nm, wherein a transition from 100% air medium to 100% silicon medium possessed a gradual refractive index (from air refractive index of 1 to silicon

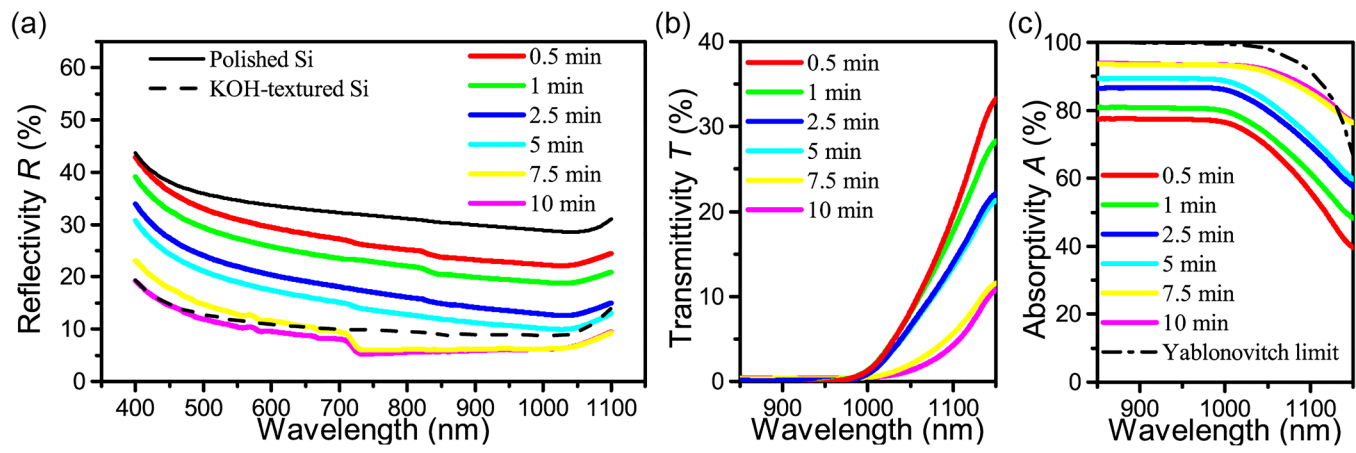


FIG. 8. (a) Reflectivity, (b) transmittivity, and (c) absorptivity of silicon wafer etched for different times using the atmospheric plasma jet.

refractive index of 3.5).⁴⁵ The optical medium effect could explain the decrease in the reflectivity of the silicon surface within a broad range of wavelengths for the initial roughening stage. In addition, the corresponding transmittivity and absorptivity in the vicinity of the silicon bandgap showed improvements. Therefore, we can deduce that the black silicon property resulting from high-frequency nanoroughness is the major reason for the increase in light trapping capability at the initial roughening stage. However, compared with the KOH-textured silicon and the Yablonovitch limit, its anti-reflectance capability can still be improved.

When the plasma etching entered the texturing stage (more than 5 min), the morphology of the silicon surface was changed to the inverted parabolic structure consisting of spherical pits. The feature width sizes of the microstructures exceeded the wavelength (approximately 1000 nm) of infrared light, and multiple reflections of the incident light took place inside the spherical pits. The average number of reflections was large when the aspect ratio of the microstructures was larger. Although the surface roughness at this stage was determined by low-frequency fluctuations, the change in microroughness did not mean that the effective medium layer disappeared or was reinforced because the intensity of the PSD function at high frequency was nearly unchanged. As shown in Fig. 9, the internal surface of the spherical pits appeared to be smooth in the morphological images but the nanoroughness of the etched surface still existed. Thus, the average reflectivity of the silicon surface etched for 7.5–10 min decreased to approximately 10%, which was equivalent to that of the KOH-textured silicon.

The transmittivity significantly decreased, especially in the wavelength range of the silicon bandgap. The corresponding absorptivity was close to the Yablonovitch limit. Moreover, an additional decline occurred at the wavelength of over 720 nm, which meant more near-infrared-light trapping. It may be explained by the light scattering at large angles because the fluctuation height of the spherical pits (approximately RMS) was in the short wavelength range of the near-infrared ray (780–1100 nm).⁹ The total internal reflection of the near-infrared light in the wafer increased the path of the incident light in the silicon, which further reduced the surface reflectance. Therefore, the etching of the second stage not only produced the microstructures with a high aspect ratio that resulted in multiple reflections of the incident light but also enhanced the optical medium effect to some extent by increasing the total effective surface area.

In summary, the silicon wafer textured by an atmospheric plasma jet possessed the dual-scale roughness features, including low-frequency fluctuations consisting of micrometer-scale structures with a high aspect ratio and the high-frequency nanoroughness that could act as an effective medium layer with a gradual refractive index. The resulting anti-reflection properties can be considered a synergy of optical medium effect and geometrical optics. In addition, the chemical and structural intactness of the light trapping structures should be reasonably evaluated because the chemical contaminations or lattice defects induced by the texturing process affect the passivation quality and the surface recombination rate of the silicon wafer.⁴⁶ In the absence of acceleration by an

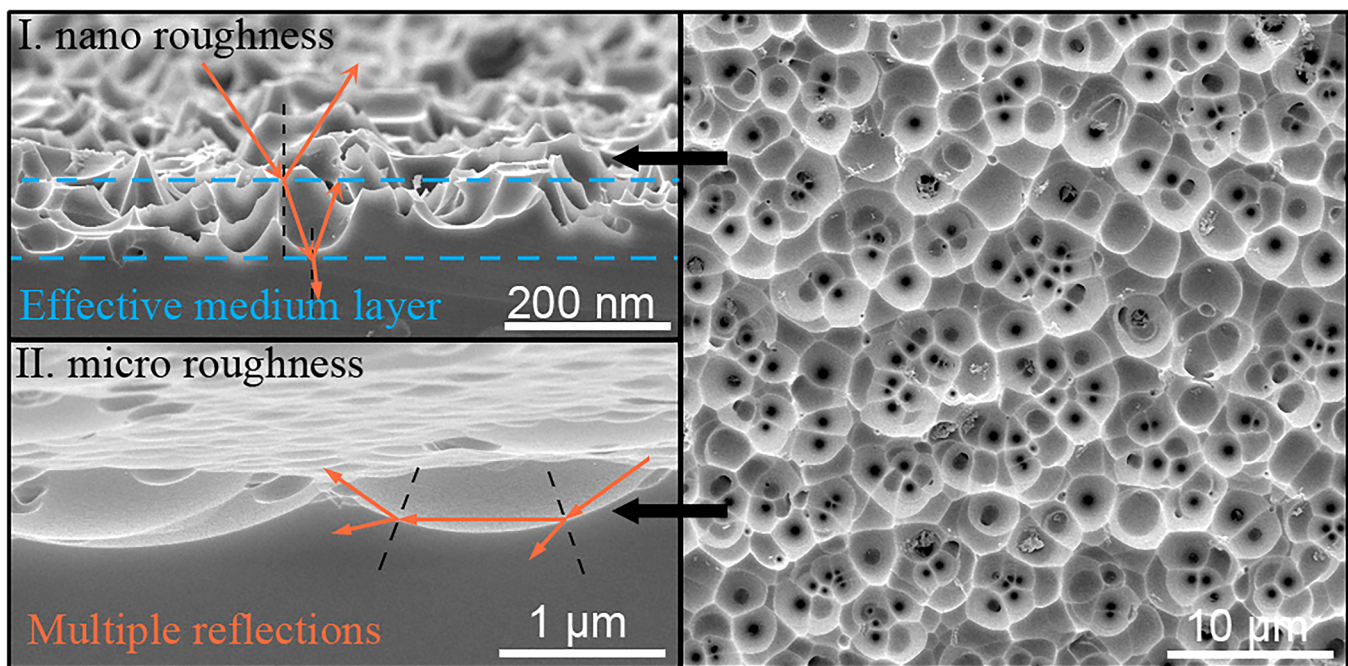


FIG. 9. SEM images of the silicon surface etched for 7.5 min by using atmospheric plasma jet. The left and right sides display cross section and top-view images, respectively.

additional voltage bias, the low-energy ions contained in a plasma jet have only a weak physical bombardment to the substrate. Atmospheric-pressure plasma etching has been proven to be a non-destructive processing method in ultra-precision optical manufacturing.⁴⁷ Thus, the marked oxidation and amorphization of the silicon surface in the atmospheric plasma etching process should have a great improvement relative to that of low-pressure RIE. With regard to the control of chemical contaminations, atmospheric-pressure plasma etching does not have an advantage because the deposition of fluorine compounds (SiO_xF_y) at the etching interface and the deep penetration of F into the Si lattice in the texturing process are always unavoidable. Although Gaudig *et al.* reported that exposure to air water molecules can facilitate the desorption of fluorine compounds,⁴⁸ the penetration depth of F^- ions into the Si lattice can still exceed 200 Å for a spontaneous etching reaction.⁴⁹ Moreover, Arora *et al.* confirmed that substrate penetration by F^- ions exerts a significant effect on the isotropic etching rate and surface roughness of silicon and probably degenerates the photovoltaic property of silicon solar cells because the diffusion of F^- ions driven by an electric field or point defects may neutralize holes and produce a *p-n* junction or even a tunnel diode.^{49,50} Therefore, to solve the issue in chemical contaminations, the penetration and diffusion mechanisms of F (or F^-) in the atmospheric-pressure CF_4/O_2 plasma etching process need to be further clarified via high-resolution transmission electron microscopy and x-ray photoelectron spectroscopy. The formation mechanism of the textured surface with dual-scale roughness and the potential electrical damages also need to be discussed in a follow-up study. Altogether, sufficient surface passivation and low surface recombination of silicon surfaces textured by atmospheric plasma is expected to be achieved via plasma-assisted atomic layer deposition of Al_2O_3 for manufacturing silicon solar cells.¹⁰ In addition, atmospheric-pressure plasma can be designed as an array of jets or a large-area dielectric barrier discharge system to provide sufficient planar space for texturing an entire cell simultaneously. Through integration into photovoltaic manufacturing lines, the production efficiency of atmospheric-pressure plasma texturing can be improved greatly.

V. CONCLUSION

An inverted parabolic light trapping structure can be obtained on the polished silicon surface via fluorine-containing atmospheric plasma etching. This approach is suitable for surface texturing of silicon solar cells due to the low surface reflectance and high fabrication efficiency without restrictions on the environment and wafer size. This study examined the etching behavior and morphology evolution of the silicon surface under given parameters conditions. The formation of the light trapping structure and the dependence of the light trapping capability on multi-scale roughness were clarified by quantitatively describing the microstructural geometrical characteristics and the roughness parameters of the etched surface. The main conclusions are summarized as follows.

- (1) The etching of atmospheric plasma jet on a smooth silicon surface is not uniform and can be considered a random selective surface roughening process. The process involves the appearance–densification–merging of micropores and the final

formation of an inverted parabolic light trapping structure consisting of spherical pits.

- (2) The formation of the light trapping structure can be divided into two stages depending on whether the original surface is completely etched or not. The morphology evolution of the etched surface was elucidated in this study from the aspects of height and spatial correlation by observing the height distribution curves, amplitude parameters, $H(r)$, and PSD functions.
- (3) The high-frequency nanoroughness of the etched surface can act as an effective medium layer with a gradual refractive index. The resulting optical medium effect causes a decline in surface reflectance within a broad range of wavelength. The low-frequency and high-amplitude microroughness originating from the spherical pits with a feature size of over 2 μm can lead to multiple reflections of the incident light and increase the total effective surface area, which further reduces the surface reflectance. The light trapping properties of textured silicon by atmospheric plasma etching are a synergy of the optical medium effect and geometrical optics.

AUTHORS' CONTRIBUTIONS

P.Z. contributed to data curation, methodology, experiments, formal analysis, writing review, and editing. J.W., H.T., and Y.D. were involved in experimental assistance and formal analysis. D.Y. was involved in conceptualization, funding acquisition, and supervision.

ACKNOWLEDGMENTS

This project was supported by the National Natural Science Foundation of China (NNSFC) (No. 52005353), the China Postdoctoral Science Foundation (No. 2020M673210), the Sichuan Science and Technology Program (No. 2020YFG0121), the Fundamental Research Funds for the Central Universities (No. 2020SCU12055), and the Miaozi Project in the Science and Technology Innovation Program of Sichuan Province (No. 20-YCG045).

DATA AVAILABILITY

The data that support the findings of this study are available within the article and are available from the corresponding author upon reasonable request.

REFERENCES

- ¹L. C. Andreani, A. Bozzola, P. Kowalczewski, M. Liscidini, and L. Redorici, *Adv. Phys. X* **4**, 1548305 (2019).
- ²Y. Rong, Y. Hu, A. Mei, H. Tan, M. I. Saidaminov, S. I. Seok, M. D. McGehee, E. H. Sargent, and H. Han, *Science* **361**, 1214 (2018).
- ³B. Radfar, F. Es, and R. Turan, *Renew. Energy* **145**, 2707–2714 (2020).
- ⁴K. A. Salman, *Solar Energy* **147**, 228–231 (2017).
- ⁵X. Tan, W. Yan, Y. Tu, and C. Deng, *Opt. Express* **25**, 14725–14731 (2017).
- ⁶D. Murias, C. Reyes-Betanzo, M. Moreno, A. Torres, A. Itzmojotl, R. Ambrosio, M. Soriano, J. Lucas, and P. R. I. Cabarracas, *Mater. Sci. Eng. B* **177**, 1509–1513 (2012).
- ⁷B. Kafle, T. Freund, A. Mannan, L. Clochard, E. Duffy, S. Werner, P. Saint-Cast, M. Hofmann, J. Rentsch, and R. Preu, *Energy Procedia* **92**, 359–368 (2016).

- ⁸M. Mews, C. Leendertz, M. Algasinger, S. Koynov, and L. Korte, *Phys. Status Solidi (RRL)* **8**, 831–835 (2014).
- ⁹M. Steglich, T. Käsebier, M. Zilk, T. Pertsch, E. Kley, and A. Tünnermann, *J. Appl. Phys.* **116**, 173503 (2014).
- ¹⁰M. Otto, M. Kroll, T. Käsebier, R. Salzer, A. Tünnermann, and R. B. Wehrspohn, *Appl. Phys. Lett.* **100**, 191603-1–191603-4 (2012).
- ¹¹B. Iandolo, A. P. Sánchez Nery, R. S. Davidsen, and O. Hansen, *Phys. Status Solidi (RRL)* **13**, 1800477 (2019).
- ¹²M. M. Plakhotnyuk, M. Gaudig, R. S. Davidsen, J. M. Lindhard, J. Hirsch, D. Lausch, M. S. Schmidt, E. Stamate, and O. Hansen, *J. Appl. Phys.* **122**, 143101 (2017).
- ¹³F. M. M. Souren, J. Rentsch, and M. C. M. van de Sanden, *Prog. Photovoltaics* **23**, 352–366 (2015).
- ¹⁴L. Bárdos and H. Baránková, *Vacuum* **83**, 522–527 (2008).
- ¹⁵D. H. Macdonald, A. Cuevas, M. J. Kerr, C. Samundsett, D. Ruby, S. Winderbaum, and A. Leo, *Solar Energy* **76**, 277–283 (2004).
- ¹⁶B. Kafle, A. I. Ridoy, P. Saint-Cast, L. Clochard, E. Duffy, K. Duncker, K. Petter, M. Hofmann, and J. Rentsch, *AIP Conf. Proc.* **1999**, 050003 (2018).
- ¹⁷J. B. Park, J. S. Oh, E. Gil, S. Kyoung, J. Kim, and G. Y. Yeom, *J. Phys. D: Appl. Phys.* **42**, 215201 (2009).
- ¹⁸D. Lausch, J. Hirscha, and N. Bernhard, “Plasma texturing of silicon wafers and finished solar cell for mass production,” *2018 IEEE 7th World Conference on Photovoltaic Energy Conversion (WCPEC) (A Joint Conference of 45th IEEE PVSC, 28th PVSEC & 34th EU PVSEC)* (IEEE, 2018).
- ¹⁹F. J. Beck, A. Polman, and K. R. Catchpole, *J. Appl. Phys.* **105**, 114310 (2009).
- ²⁰W. Guo, S. K. Anantharajan, X. Zhang, and H. Deng, *J. Micro Nano Manuf.* **8**, 024501 (2020).
- ²¹H. Paetzelt, G. Böhm, and T. Arnold, *Plasma Sources Sci. Technol.* **24**, 025002 (2015).
- ²²B. T. Chan, E. Kunnen, K. Xu, W. Boullart, and J. Poortmans, *IEEE J. Photovoltaics* **3**, 152–158 (2013).
- ²³P. Panduranga, A. Abdou, Z. Ren, R. H. Pedersen, and M. P. Nezhad, *J. Vac. Sci. Technol. B* **37**, 061206 (2019).
- ²⁴S. Kim, J. Park, J. Kim, C. Kim, and J. Kim, *ECS J. Solid State Sci. Technol.* **8**, Q76–Q79 (2019).
- ²⁵M. Moreno, D. Daineka, and P. R. I Cabarrocas, *Sol. Energy Mater. Sol. Cells* **94**, 733–737 (2010).
- ²⁶I. Zubel and M. Kramkowska, *Sens. Actuators A* **115**, 549–556 (2004).
- ²⁷P. Papet, O. Nichiporuk, A. Kaminski, Y. Rozier, J. Kraiem, J. F. Lelievre, A. Chaumartin, A. Fave, and M. Lemiti, *Sol. Energy Mater. Sol. Cells* **90**, 2319–2328 (2006).
- ²⁸P. Wang, S. Xiao, R. Jia, H. Sun, X. Dai, G. Su, and K. Tao, *Solar Energy* **169**, 153–158 (2018).
- ²⁹K. M. Park, M. B. Lee, and S. Y. Choi, *Sol. Energy Mater. Sol. Cells* **132**, 356–362 (2015).
- ³⁰D. Payne, M. Abbott, A. Lopez, Y. Zeng, T. Fong, K. McIntosh, J. Cruz-Campa, R. Davidsen, M. Plakhotnyuk, and D. M. Bagnall, “Rapid optical modelling of plasma textured silicon,” *European Photovoltaic Solar Energy Conference (EU PVSEC, 2017)*.
- ³¹D. Abi Saab, P. Bassett, M. J. Pierotti, M. L. Trawick, and D. E. Angelescu, *Phys. Rev. Lett.* **113**, 265502 (2014).
- ³²D. Murias, M. Moreno, C. Reyes Betanzo, A. Torres, P. Rosales, J. Martínez, R. Ambrosio, P. R. I Cabarrocas, N. Carlos, and A. Itzmojotl, *Phys. Status Solidi (a)* **213**, 1937–1941 (2016).
- ³³J. Hirsch, M. Gaudig, N. Bernhard, and D. Lausch, *Appl. Surf. Sci.* **374**, 252–256 (2016).
- ³⁴A. Schutze, J. Y. Jeong, S. E. Babayan, R. F. Hicks, J. Park, and G. S. Selwyn, *IEEE Trans. Plasma Sci.* **26**, 1685–1694 (1998).
- ³⁵M. J. Johnson, D. R. Boris, T. B. Petrova, and S. G. Walton, *IEEE Trans. Plasma Sci.* **47**, 434–444 (2019).
- ³⁶M. Gaudig, M. Maiberg, M. Plapp, and R. B. Wehrspohn, *J. Appl. Phys.* **124**, 233302 (2018).
- ³⁷F. Kaule, B. Köhler, J. Hirsch, S. Schoenfelder, and D. Lausch, *Sol. Energy Mater. Sol. Cells* **185**, 511–516 (2018).
- ³⁸P. Zhang, C. Chen, C. Xiao, L. Chen, L. Jiang, and L. Qian, *Tribol. Int.* **128**, 174–180 (2018).
- ³⁹J. Wu, P. Zhang, D. Yu, S. Zhang, Q. Xin, and Y. Wan, *Optik* **214**, 164815 (2020).
- ⁴⁰G. Boulousis, V. Constantoudis, G. Kokkoris, and E. Gogolides, *Nanotechnology* **19**, 255301 (2008).
- ⁴¹E. Gogolides, *Microelectron. Eng.* **73–74**, 312–318 (2004).
- ⁴²N. Nakazaki, H. Matsumoto, H. Tsuda, Y. Takao, K. Eriguchi, and K. Ono, *Appl. Phys. Lett.* **109**, 204101 (2016).
- ⁴³E. Yablonovitch, *J. Opt. Soc. Am.* **72**, 899 (1982).
- ⁴⁴M. A. Green and M. J. Keevers, *Prog. Photovoltaics* **3**, 189–192 (1995).
- ⁴⁵R. B. Stephens and G. D. Cody, *Thin Solid Films* **45**, 19–29 (1977).
- ⁴⁶B. Iandolo, A. P. Sánchez Nery, R. S. Davidsen, and O. Hansen, *Phys. Status Solidi (RRL)* **13**, 1800477 (2019).
- ⁴⁷Q. Xin, X. Su, and B. Wang, *Appl. Surf. Sci.* **382**, 260–267 (2016).
- ⁴⁸M. Gaudig, J. Hirsch, V. Naumann, M. Werner, S. Großer, C. Hagendorf, N. Bernhard, and D. Lausch, *J. Appl. Phys.* **121**, 063301 (2017).
- ⁴⁹H. F. Winters, D. B. Graves, D. Humbird, and S. Tougaard, *J. Vac. Sci. Technol. A* **25**, 96–103 (2007).
- ⁵⁰P. Arora, T. Nguyen, A. Chawla, S. Nam, and V. M. Donnelly, *J. Vac. Sci. Technol. A* **37**, 061303 (2019).